Food Chemistry: X 23 (2024) 101604

Contents lists available at ScienceDirect

Food Chemistry: X

journal homepage: www.sciencedirect.com/journal/food-chemistry-x

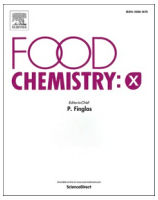

Synthesis, characterization, antioxidant and bacteriostasis in preservation of isoorientin loaded Zein/GA nanoparticles

Yuxia Yang [1], Yingyu Jia [1], Meng Zhang [1], Ying Luo, Zhong Zhang, Wanqiang Wu, Li Yuan [*]

Engineering Research Center of High Value Utilization of Western China Fruit Resources, College of Food Engineering and Nutritional Science, Shaanxi Normal University, Xi'an 710119, People's Republic of China

ARTICLE INFO

Keywords:
Nanoparticle
Structural characterization
Stability
Antioxidant activity
Antibacterial activity

ABSTRACT

Isoorientin (Iso) is a natural flavone with multiple activities. In the present study, the partial chemical properties and activities of Iso were improved by the nanoparticle loading technique. Zein/GA nanoparticles were successfully synthesized with the antisolvent precipitation method, and the structure and stability of the Zein/GA nanoparticles loaded with Iso (Zein/GA-Iso nanoparticles) were characterized by FTIR, UV–vis spectroscopy and zeta-sizer analysis. Results showed that Zein/GA-Iso nanoparticles possessed greater stability, light stability, hydrophilicity and antioxidant activity. Furthermore, Zein/GA-Iso nanoparticles exerted notable antibacterial activity against *E. coli, S. aureus,* and *P. aeruginosa* by destroying the permeability and integrity of cell membrane. On this basis, Zein/GA-Iso nanoparticles do have a bacteriostatic effect on pork. In conclusion, Zein/GA-Iso nanoparticles had better stability and pork preservation for applications in the food processing field as a new type of antiseptic and freshening agent.

1. Introduction

Isoorientin (Iso) is a natural flavonoid that has received widespread attention owing to its excellent biological effects, such as antioxidant activity (Lim et al., 2007), anti-inflammatory activity (Yuan et al., 2014), and anti-cancer activity (Lin et al., 2016). Iso possesses a broad-spectrum antibacterial effect (Ambika & Sundrarajan, 2015) with the high safety for human consumption. However, its application is limited due to poor water solubility and chemical instability. To overcome these shortcomings and enhance the efficacy of natural active substances, a variety of delivery systems has been designed, including nanoparticles, hydrogels and liposomes. Among these delivery systems, nanoparticles offer the unique advantages such as smaller particle size, high safety, and good slow-release effect. Nanoparticles are defined as particles with sizes smaller than 1000 nm in the biological sciences (Antônio et al., 2016). Using nanotechnology, active molecules such as tocopherols, quercetin curcumin, *etc.* can be converted into nanoparticles that are stable across a wide range of pH, temperature, and ionic strength. Encapsulation Iso in the nanoparticles delivery systems is an effective way to promote water solubility and stabilization of Iso.

In recent years, because of the strong binding ability with bioactive compounds, high safety, simple preparation, and good biocompatibility, proteins have usually been used as a potential nanocarrier to deliver natural compounds (Gagliardi et al., 2021), such as wheat gliadin, bovine serum albumin, and whey protein.

Zein exhibits inherent hydrophobicity because of its higher proportions of hydrophobic amino acid residues (>50%). Zein usually forms uniform and spherical nanoparticles in water at a certain stirring rate due to its unique hydrophobicity and self-assembly characteristics (Zhang et al., 2022). However, Zein nanoparticles have the disadvantage of poor stability because of its strong hydrophobicity (Gali et al., 2022). Some studies have found that gum arabic, pectin, chitosan, soybean polysaccharides (Gao et al., 2021) can crosslink with zein as stabilizers to improve the stability of Zein nanoparticles.

Gum Arabic (GA) is a complex heteropolysaccharide, which exists in the form of a neutral or weakly acidic salt, the protein portion accounts for about 2% of the total gum, and polysaccharides are covalently bonded to protein peptide chains though hydroxyproline and serine connection. It has been reported that adding GA to Zein nanoparticles (compared to pure Zein nanoparticles) significantly enhances their stability against pH variations (in the range 2–8), ionic strength (in the range 25–100 mM at pH 4), and heating up to a temperature of 100 °C,

* Corresponding author at: Xi'an, Shaanxi 710119, China.
E-mail address: yuanli112086@snnu.edu.cn (L. Yuan).
[1] Author Contributions: Y. J. and M. Z. contributed equally to this work.

https://doi.org/10.1016/j.fochx.2024.101604
Received 13 April 2024; Received in revised form 23 June 2024; Accepted 28 June 2024
Available online 1 July 2024

likely due to the formation of a complex nanoparticle structure. Some studies have suggested that GA adsorbs onto the surface of Zein nanoparticles through electrostatic and hydrophobic interactions, enhancing the stability of Zein/GA nanoparticles used for delivering active substances such as curcumin, tocopherol, thyme essential oil, *etc.* However, no delivery system application for Iso has been reported yet.

The purpose of this study is to form Zein/GA nanoparticles by the classical antisolvent precipitation method as the carrier to load Iso. Exposure to challenging environmental conditions during food processing, storage, cooking or passage through the gastrointestinal tract could significantly affect nanoparticle size, structure, and charge, and consequently impact the capacity of bioactive substance. Therefore, the structural characterization and stability under various conditions including pH levels, salt solutions, *in vitro digestion*, temperature, storage and light exposure of Zein/GA-Iso nanoparticles were investigated in this study. Besides, the antioxidant properties, cytotoxicity, and antibacterial activity of the Zein/GA-Iso nanoparticles were also evaluated. The findings of this study will provide valuable references for the utilization of Iso and the delivery systems of natural bioactive compounds.

2. Experimental procedures

2.1. Materials

Iso (purity≥98%) was obtained from Pharmaceutical Technology Co., Ltd. (Jiangsu China). Zein (protein content 91.3%) and GA powder (99%) were obtained from Fuchen Chemical Reagents Co., Ltd. (Tianjin, China). Pig bile salts were acquired from Beijing Ao boxing Bio-tech Co., Ltd. (Beijing, China). Pepsin (activity 3000–3500 U mg^{-1}), Lipase (TypeII, 100–500 Umg^{-1} protein, 30–90 Umg^{-1} protein), Pancreatin(8× USP specifications), Trypsin (activity 250 USP Umg^{-1}) rom porcine pancreas and Mucins (TypeIII) from porcine stomach were purchased from Sigma-Aldrich (Shanghai China) Trading Co. Ltd. Human colorectal adenocarcinoma Caco-2 cells and the human HL-7702 hepatocyte cells were purchased from the Fourth Military Medical University (Xian, China).

2.2. Preparation of Zein/GA nanoparticles

Zein/GA nanoparticles were prepared by the antisolvent precipitation method (Song et al., 2020. Fig. 1A). Briefly, at room temperature, 2.0 g of GA was dissolved in 10 mL deionized water with magnetic stirring at 600 rpm for 1 h to prepare the GA stock solution at room temperature. 1.0 g of Zein dissolved in 20 mL 70% (*v*/v) aqueous ethanol solution with magnetic stirring at 600 rpm for 0.5 h. Then, Zein solution stock was taken and dispersed in a thin flow in deionized water, and 300 μL of GA stock solution was added to the above-deionized water in a trickle and stirred with a magnetic stirrer at 600 rpm for 2 h. The pH of the sample was adjusted to 4 and then centrifuged at 4000*g* for 10 min. Finally, the suspensions are for freeze-drying, and the rest are stored at 4 °C.

2.3. Preparation of Zein/GA-Iso nanoparticles

0.01 g of Iso was taken and dissolved in 5 mL Zein stock solution (the ratio of Iso to Zein is 1:10) and heated to 40 °C to fully mix. The suspensions were adjusted to pH 4 and centrifuged at 4000*g* for 10 min. Freeze dry and weigh the freshly prepared nanoparticles. Percent Zein/GA-Iso nanoparticles determination of acquisition efficiency was determined using the following formula (1):

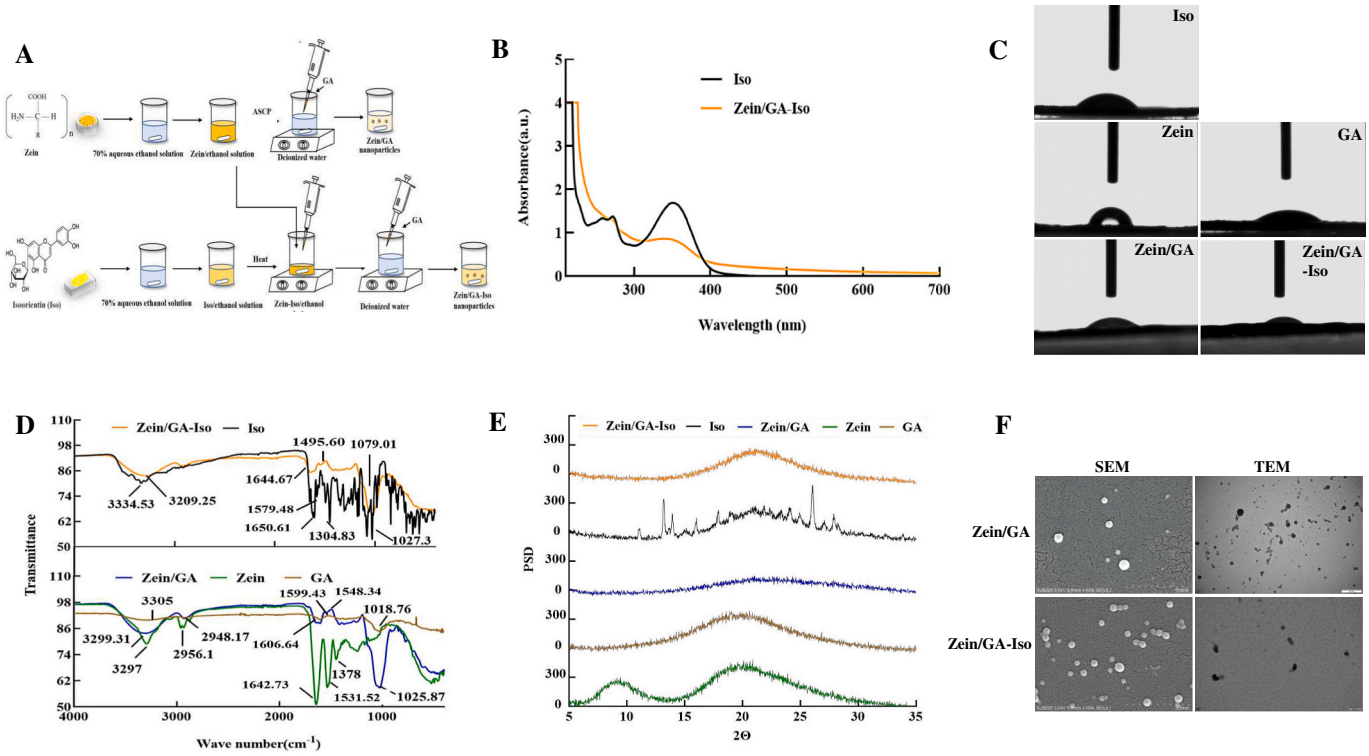

Fig. 1. The synthesis pathways and structural characterization of Zein/GA-Iso nanoparticles.
(A) Zein/GA and Zein/GA-Iso nanoparticles synthesis pathways. (B) UV spectra of Iso and Zein/GA-Iso nanoparticles. (C) Water contact angle of zein, GA, Iso, Zein/GA and Zein/GA-Iso nanoparticles. (D) FT-IR analysis of zein, GA, Iso, Zein/GA and Zein/GA-Iso nanoparticles. (E) XRD of Iso, zein, GA, Zein/GA and Zein/GA-Iso nanoparticles. (F)SEM and TEM images of Zein/GA and Zein/GA-Iso nanoparticles.

$$\text{Yield}\ (\%) = [\text{Freeze dried of Zein/GA} - \text{Iso}\ (\text{mg}) / \text{Sum of weight of zein, GA, and Iso}\ (\text{mg})] \times 100\% \quad (1)$$

2.4. Iso loading efficiency determination

Zein/GA-Iso nanoparticles were dispersed in an 80% ethanol-water solution(*v*/v) and take the same Zein/GA-Iso nanoparticles and disperse in water at 90 °C through vortex oscillation for 2 min respectively. Each of the samples were centrifugated at a speed of 10,000*g* for 15 min and the supernatant was collected. Absorbance was measured with a UV–visible spectrophotometer at 350 nm. The Iso loading efficiency was calculated by following eq. (2):

$$\text{Iso loaded}\ (\%) = (\text{Amount of Iso loaded/Total Iso used}) \times 100\% \quad (2)$$

2.5. Characterization of Zein/GA nanoparticles and Zein/GA-Iso nanoparticles

2.5.1. Measurement of average particle size and zeta potential

The mean size and zeta potential of Zein/GA and Zein/GA-Iso nanoparticles were measured through a zeta sizer (ZEN3690, Malvern instrument, UK). The concentration of the prepared samples of nanoparticles was diluted 10 times by using water as a dispersant before detecting at 25 °C.

2.5.2. UV–vis spectroscopy measurement

The Iso and Zein/GA-Iso nanoparticles were dissolved in 70% ethanol respectively, and 70% ethanol was used as blank control and scanned in the wavelength range of 0–700 nm.

2.5.3. FTIR and XRD

Fourier transforms spectrophotometer (Shimadzu, Kyoto) was used to detect the chemical construction of nanoparticles in a range of 400–4000 cm^{-1}. 5 mg sample was weighed and mixed them with 500 mg KBr (samples: KBr = 1:100). Before being measured, the mixtures were then pressed into sheets and placed on a sample stand. The XRD patterns were used through an X-ray diffractometer (Bruker, D8 Advance, Germany) to determine the structure of samples. The scan rate was 4°/min, and the scanning angle (2θ) was from 5°to 90°.

2.5.4. SEM and TEM observation

A small amount of freeze-dried sample power was fixed with a double-sided conductive adhesive. Before imaging, the samples were coated with a conductive gold layer by a carbon coater for 50 s. Next, photographs were taken with SEM (FEI, Nava NanoSEM 450, Czech Republic) at an accelerating voltage of 15.0 kV. Nanoparticles of redissolved solutions were respectively taken to the carbon-coated copper grid. The prepared samples were characterized by TEM (FEI, Tecnai G2 F20, Japan) after the samples were dried at 20 °C for 24 h.

2.5.5. Contact angle

Samples were pressed into tablets with a tablet press. The samples were placed on the slide and fixed on the test platform, dropped a drop of distilled water on the surface of the samples, and at last record the contact angle data with a contact angle tester (Kruss, KRUSS-DSA100, Germany).

2.6. Chemical stability assessment

2.6.1. Effect of pH and ionic strength on the stability of nanoparticles

The pH of freshly prepared nanoparticles was about 5, adjusted pH to 2, 4, 6, 8, and 10 with 1 M HCl and 1 M NaOH, respectively. Nanoparticles were dispersed in deionized water with pH 4, 1 M NaCl was added to obtain samples with different concentrations and measured after standing at 25 °C for 2 h. The influence of pH and ionic strength on nanoparticles stability was determined by measuring the mean size and zeta (ZEN3690, Malvern instrument, UK) at different pH values and ionic strength, respectively.

2.6.2. Effects of the simulated digestion system in vitro on the stability of nanoparticles

Nanoparticles were passed through a three-stage simulated gastrointestinal tract model (mouth, stomach, and small intestinal stages), and were evaluated by measuring the change of the mean size and zeta potential of nanoparticles at different stages.

Initial system: 10.00 mL Zein/GA nanoparticle and Zein/GA-Iso nanoparticles solution were dissolved in deionized water. 20 mL of the solution was put into a water bath at 37 °C preheating and placed in a shaker at 130 rpm with 37 °C for 10 min.

Mouth phase: The nanoparticles solution(0.5 mg/mL)and mucin solution (0.03 g/mL) were mixed in a volume ratio of 1:1, adjusted to pH 6.8 and placed in an incubator shaker at 37 °C with 130 rpm for 10 min.

Stomach phase: The artificial gastric juice system was prepared by adding 0.4 g NaCl and 1.4 mL 1 M HCl in 200 mL deionized water. 20 mL samples collected after digestion in the mouth phase were mixed with 20 mL simulated gastric fluid and 0.64 g pepsin, adjusted to pH 2 and reacted in an incubator shaker at 100 rpm with 37 °C for 2 h.

Small intestinal phase: The pH of Zein/GA nanoparticle solution and Zein/GA-Iso nanoparticle solution was adjusted to 7.5 by NaOH to stop gastric digestion. Gastric digestion mixture was mixed with the simulated intestinal digestive juice (0.3 mM $CaCl_2$, 30.72 mM NaCl, 5 mg/L bile salt into 200 mL deionized water) at the volume ratio of 1:1, adjusted pH to 7, added 8 mg/mL pancreatin. Then, the digestive juice was placed in a shaker and incubated at 130 rpm (37 °C) for 2 h.

2.6.3. Effect of heating and storage time on the stability of nanoparticles

Nanoparticles were divided into four equal parts and heated in a water bath to 0 °C, 20 °C, 50 °C, 90 °C for 1 h, respectively, then were cooled down to 25 °C. For storage time: nanoparticles were stored in a refrigerator at 4 °C for 12 h, 24 h, 38 h, and 48 h. The mean size and zeta potential were measured to evaluate the stability of the samples.

2.6.4. Effect of UV light on the stability of Iso and Zein/GA-Iso nanoparticles

Equal amounts (10 mL) of Iso solution (0.5 mg/mL 70% ethanol) and Zein/GA-Iso dispersion (0.5 mg/mL 70% ethanol) were placed in separate petri dishes. The Iso concentrations were measured at 350 nm with a microplate reader every 15 min after UV light irradiation at 365 nm for 1 h.

2.6.5. Bioavailability of Iso and Zein/GA-Iso nanoparticles

After incubating the nanoparticle solution in a water bath at 37 °C for 15 min, it was fully mixed with simulated gastric fluid in a volume ratio of 1:1, and the pH was adjusted to 2. Subsequently, the mixture was simulated digested at 37 °C with 100 rpm for 2 h. Mix the solution digested in the stomach with intestinal fluid evenly at a ratio of 1:1, and quickly adjusted the pH to 7. The mixed solution was digested for 3 h at 270 rpm at 37 °C. Preparation of Iso standard curve by HPLC (Agilent, Shimadzu, Japan). Gadient elution at 25 °C with a flow rate of 1.0 mL/min, and monitored using UV at 350 nm. ISO standard (purity ≥98%) was obtained from Pharmaceutical Technology Co., Ltd. (Jiangsu China). The concentration of the sample solution taken out from the two digestions was determined under the same chromatographic conditions, and the bioavailability of Iso and Zein/GA-Iso nanoparticles were calculated using formula (3):

$$\text{Bioavailability}\ (\%) = C \times V/M \times 100\% \quad (3)$$

The C refers to the Iso concentration (mg/mL) obtained by digestive fluid in stomach and intestinal respectively, the V is volume of digestive fluid, and M means the mass of Iso in the zein/GA-Iso.

2.7. In vitro antioxidant assay

2.7.1. DPPH and ABTS$^+$ radical scavenging capacity

Iso and Zein/GA-Iso nanoparticles (50 μL) were fully mixed with freshly prepared DPPH (0.1 mM in absolute ethanol) and then reacted for 30 min in the dark. The absorbance (A_1) was measured at 517 nm with a microplate reader. The absorbance of deionized water mixed with DPPH solution was also measured as the blank (A_0). Absolute ethanol was used instead of DPPH solution as the control group (A_2). DPPH radical scavenging rate according to formula (4):

$$\text{Scavenging rate}\ (\%) = 1\text{–}(A_1\text{–}A_2/A_0 \times 100\% \quad (4)$$

ABTS was mixed with potassium persulfate ($K_2S_2O_8$) to 7.0 mM and 2.45 mM, respectively. The samples were allowed to react with the ABTS$\bullet^+$ solution for 6 min in the dark, and the absorbance (A_1) was measured at 734 nm. In the blank group (A_0), deionized water was used instead of sample, and the above operations were repeated. The control group used deionized water instead of ABTS$\bullet^+$ solution as A_2. ABTS$\bullet^+$ radical scavenging rate was calculated according to the formula (5):

$$\text{Scavenging rate}\ (\%) = 1\text{–}(A_1\text{–}A_2/A_0 \times 100\% \quad (5)$$

A1 - absorbance value of the measurement group.
A0 - absorbance value of blank group.
A2 - absorbance value of control group.

2.7.2. Effect on hemolysis of red blood cells and cytotoxicity

The red blood cells were collected from the blood of SPF healthy 6-week-old male BALB/c mice from the Experimental Animal Center of Xi ‘an Jiaotong University (Xian, China). The blood of the mouse was centrifuged at 3000 rpm for 10 min, and the supernatant was discarded to get a precipitate of red blood cells. Sample solution was added 100.0 μL of 0.5% red blood cell suspension, then H_2O_2 (the solution concentration of 2%) was added. After incubating at 37 °C for 1 h, centrifuged at 3000 rpm for 5 min, finally, the supernatant was taken to measure the absorbance at 540 nm. The hemolysis inhibition rate was calculated according to formula (6):

$$\text{Inhibition rate}\ (\%) = (\text{A control} - \text{A sample})/(\text{A control} - \text{A blank}) \times 100\% \quad (6)$$

Acontrol - absorbance value of the control group.
Asample - absorbance value of sample group.
Ablank - absorbance value of blank group.

Briefly, 2×10^5 cells were inoculated into 96 well plates, and cultured in the incubator at 37 °C with 5% (*v*/v) of CO_2 for 24 h. 100 μL of treated samples which was freshly configured solutions of Iso and Zein/GA-Iso nanoparticles with different concentrations (25, 50, 100 and 200 μg/mL) were added to the wells. After 12 h of incubation, 10 μL of CCK-8 solution (Shanxi Bio Bio Biotechnology Co, Ltd., Shanxi, China) was added and incubated for 1 h. Subsequently, the absorbance was measured at 450 nm with a microplate reader. Cell viability was calculated by the formula (7):

$$\text{Cell viability}\ (\%) = [A_1 - A_0]/[A_2 - A_0] \times 100\% \quad (7)$$

Additionally, after treatment, the fluorescence of intracellular Reactive oxygen species (ROS) was observed under Fluorescence microscope (Olympus Optical, Tokyo, Japan) or Flow cytometer (Partec GmbH, Münster, Germany).

2.8. Antibacterial activity of nanoparticles

The single colonies of *Escherichia coli* (*E. coli*), *Pseudomonas aeruginosa* (*P. aeruginosa*), *Staphylococcus aureus* (*S. aureus*) was cultured on a constant temperature shaker for 24 h (37 °C, 110 rpm). Dilute the bacterial suspension to 10^6 -10^7 CFU/mL with sterile physiological saline.

2.8.1. Bacteriostatic circle and bacteriostatic rate assay

Prepare sterile 6 mm diameter filter paper and place it in the configured sample solution for 12 h. Evenly coat the bacterial suspension on the solid culture medium. Place the prepared drug-sensitive paper pieces on the solid culture medium, sterile water as the blank control, and culture them in a constant temperature incubator at 37 °C for 24 h. The obtained of bacteriostatic circle whose size was measured by a vernier caliper. Calculate the bacteriostatic rate using the following formula (8):

$$\text{Bacteriostatic rate}\ (\%) = (\text{Lsample} - \text{Lcontrol})/\text{Lsample} \times 100\% \quad (8)$$

Lsample- diameter of the circle of inhibition of the sample group.
Lcontrol-diameter of the inhibition circle of the controlm group.

2.8.2. Minimal inhibition concentration

The minimum inhibitory concentration (MIC) of the samples was determined by the evaluated double dilution method (Wiegand et al., 2008). Dilute the sample solution with LB liquid (Tianjin Tianli Reagent Co., Ltd., Tianjin, China) medium as follows 800, 400, 200, 100, 50 μg/mL. 100 μL of the bacterial suspension (10^3–10^4 CFU/100 μL) was added to the diluted samples and were incubated at 37 °C for 15 h in a thermostatic incubator with a vibration rate of 110 r/min. After it was continuously cultured for 15 h was inoculated on LB solid medium by scribing and observing.

2.8.3. Growth curve

2.0 mL of Iso, Zein/GA nanoparticle and Zein/GA-Iso nanoparticle solutions were added to 12 mL of LB liquid medium respectively to adjust their concentration to the MIC. And then 100.0 μL of the bacterial suspension was connected. Culture for 24 h continuously (37 °C,110 rpm), and take samples every 2 h to measure the absorbance at 600 nm.

2.8.4. Membrane permeability of bacterial cells

The sample suspension was adjusted to the concentration of MIC by LB liquid medium. And then 100.0 μL of the bacterial suspension was connected. The samples were incubated at 37 °C, 120 r/min for 10 h in a constant temperature oscillating incubator, and the control group used sterile secondary water instead of sample solution. The samples were taken at an interval of 2 h each time. After centrifugation at 3500 *g* for 15 min, the protein content of supernatant was determined by the BCA kit (Xi'an Aorui Jingchuang Biotechnology Co. Ltd. Shaanxi, China). The absorbance of the supernatant was measured at 260 nm and the membrane permeability of bacterial cells was determined by the conductivity of bacterial solutions.

2.8.5. Imaging of bacteria by SEM

Iso and Zein/GA-Iso nanoparticles were prepared in LB liquid medium with the concentration of MIC, and then 200.0 μL of bacterial suspension (2×10^3–2×10^4 CFU/100 μL) was added, then incubated in a constant temperature shaking incubator for 10 h (37 °C, 120 r/min), and then centrifuged at 3500 *g* for 10 min, the supernatant was discarded, the precipitate was retained and washed with PBS repeatedly. The washed bacterial precipitate was pelleted and fix the bacteria on the conductive carbon adhesive, gold-coated with an ion sputter for 30 s, and observed at the 3.0 kV instrument voltag.

2.9. Preservation effect of Zein/GA-Iso nanoparticles on chilled meat

2.9.1. Sample pretreatment

Fresh pork was bought in the supermarket of Shaanxi normal

Table 1
The mean size, PDI, and Zeta potential of zein/GA and zein/GA-Iso with the % Iso loading efficiency.

Groups	Mean size (nm)	Index of polydispersion (PDI)	Zeta potential (mV)	Yield of nanoparticles (%)	Iso load rate (%)
Zein/GA	122.21 ± 0.87	0.29 ± 0.01	−36.57 ± 0.72	75.56	
Zein/GA-Iso	149.31 ± 2.13	0.31 ± 0.01	−55.21 ± 0.64	78.89	67.56

University (Xian, China). First of all, remove the fat and connective tissue from the surface of chilled meat, cut it into uniform blocks (3 cm × 3 cm × 2 cm) and divide it into four parts. The samples were soaked in aseptic secondary water, 0.05% Iso, zein/GA nanoparticles and zein/GA-Iso nanoparticles, respectively, and the experiments were repeated three times in each group. The treated samples were drained, wrapped in plastic film and stored at 4 °C. The pH, juice loss rate, texture, color difference, volatile saline nitrogen content, and total colony indexes of samples in each group were detected and observed on 0,2,4,6,8,10,12,14 days respectively.

2.9.2. Determination of pH

According to GB 5009.237–2016 "Food pH determination". Fresh pork was pulverized into homogeneous meat samples using a grinder, and added 10 times KCL solution while mixing and homogenizing. The pH of the samples was determined using a hand-held pH meter.

2.9.3. Determination of juice loss rate

The pork was packaged and weighed in groups, labeled W_1, and the package was slowly opened before the index determination, and the liquid on the surface of the meat sample was drained with sterile filter paper, labeled W_2. The juice loss rate (%) of pork is calculated according to the following formula (9):

$$\text{Juice loss rate}(\%) = \frac{W_1 - W_2}{W_1} \quad (9)$$

2.9.4. Determination of color difference

The color difference of meat samples after treatment was determined by a color difference meter (Shenzhen SUNSHI Technology Co., Ltd., Shenzhen, China). The black and white standard block of the colorimeter was used to correct equipment. Samples were randomly collected from 3 locations on the surface of meat samples, and L* (brightness), a* (red) and b* (yellow) values of the blank control group, Iso and zein/GA-Iso nanoparticle groups were determined.

2.9.5. Determination of volatile base nitrogen content

According to GB5009.228–2016 "Determination of volatile base nitrogen in food under National Food Safety Standard". Briefly, 20 g of pork samples were stirred and placed in a conical flask, added 100 mL of sterile deionized water, then were shaken for 30 min, filtered, the residue was discarded and the filtrate was collected. The content of TVB-N in pork was determined by an automatic Kjeldahl nitrogen analyzer.

2.9.6. Determination of total number of colonies

Method Refer to GB 4789.2–2010 "Determination of Total colonies".10 g of meat samples were mixed well in 100 mL of sterile saline, 1 mL of suspension was diluted according to the results of the pre-experiment, evenly coated, incubated for 48 h and observed the plate and counted in log cfu/g.

2.10. Statistical analysis

All experiments were repeated at least three times, and the results were presented as the mean ± standard deviation (SD). The GraphPad Prism version 6.0 software was used to analyze the statistical significance with one-way ANOVA, and $p < 0.05$ was considered as a significant difference.

3. Results

3.1. Synthesis of Zein/GA and Zein/GA-Iso nanoparticles

The yield of Zein/GA and Zein/GA-Iso was 75.6% and 78.9%, respectively, and the loading efficiency of Iso in Zein/GA nanoparticles was 67.6% (Table 1). As shown in Fig. 1B, the UV visible spectrum analysis confirmed that the maximum absorption wavelength of Iso was mainly at 350 nm. However, the decrease in the peak intensity of Zein/GA-Iso complexes indicated the formation of the amorphous complexes, suggesting an intermolecular interaction occurred between Zein/GA and Iso.

3.2. Structural characterization of nanoparticles

As shown in Fig. 1C, the contact angles of zein, GA, and zein/GA nanoparticles are 90.6°, 36°, and 33.5°, respectively. These results indicated that the hydrophilicity of zein/GA nanoparticles is significantly improved after electrostatic interaction. The contact angle of Iso and Zein/GA-Iso nanoparticles was 38.9° and 27.3°, respectively, indicating that the hydrophilicity of Iso was significantly improved by loading on Zein/GA nanoparticles.

In FTIR curve (Fig. 1D), the first characteristic peak of Iso appeared at 3334.53 cm^{-1}, and the peak of Zein/GA-Iso nanoparticles showed a red shift (from 3299 cm^{-1} to 3209 cm^{-1}) compared with Zein/GA-Iso nanoparticles, suggesting that the hydrogen bonds may be formed between amide groups of the glutamine in Zein and hydroxyl groups in GA (Li et al., 2019). Hydrogen bonds as a driving mechanism may be responsible for the formation of Zein/GA nanocomposites. The second characteristic absorption peak was stretching vibration at 1500–1700 cm^{-1}. These stretching vibration peaks of Zein were at 1642.73 cm^{-1} and 1531.52 cm^{-1} representing amide I (C═O stretching), and amide II (C—N stretching) bonds, respectively. For the spectrum of GA, the band at 1599.43 cm^{-1} was considered as stretching of C═C. The characteristic peaks of Iso were 1650.61 cm^{-1} and 1579.48 cm^{-1}, which were attributed to the stretching vibration of C═O and C═C. The peaks of Zein/GA nanoparticles shifted to 1606.64 cm^{-1} and 1548.34 cm^{-1}. As compared to the peak of Zein, the stretching vibration peaks of amide I red-shifted, and the peaks of amide II blue-shifted, which revealed the hydrophobic force and electrostatic interactions occurred between Zein and GA. However, for Zein/GA-Iso nanoparticles, two peaks of amide I and II band were shifted to 1644.67 cm^{-1} and 1495.60 cm^{-1}, which indicated the electrostatic interactions and hydrophobic force existed in the formation of Zein/GA-Iso nanoparticles. The possible explanation was that the assembly behavior of zein molecules is determined by the associative hydrophobic interactions, which can be altered by the polarity of the solvent (Wang & Padua, 2010).

As shown in Fig. 1E, some characteristic peaks of free Iso were at 11.21°, 13.15°, 14.30°, 16.21°, 19.87°, 26.3°, 28.7°, representing that Iso was a crystal structure. Two characteristic peaks of Zein were at 9.31° and 20.71°, which verified that the protein was amorphous. Further, Zein/GA nanoparticles were also observed to be amorphous, while Zein/GA-Iso nanoparticles only detected a wide characteristic peak at 22.35°, indicating that the characteristic peak of the crystal disappeared after the successful loading of Iso onto Zein/GA nanoparticles.

As shown in Table 1, the mean size of the Zein/GA nanoparticles was 122.21 ± 0.87 nm with (Polydispersity Index) PDI = 0.29 ± 0.01, and

Zein/GA-Iso nanoparticles was 149.31 ± 2.31 nm with PDI = 0.31 ± 0.01. Both the mean size and PDI increased after loading Iso. The zeta potential of Zein/GA and Zein/GA-Iso nanoparticles was around −36.57 mV and − 55.21 mV, respectively. Similarly, the zeta potential of Zein/GA-Iso nanoparticles was lower than that of Zein/GA nanoparticles, indicating that Zein/GA-Iso nanoparticles were more stable than Zein/GA. Additionally, both Zein/GA and Zein/GA-Iso nanoparticles were spherical with a smooth surface (Fig. 1F), and the mean size of Zein/GA-Iso nanoparticles was slightly larger than that of Zein/GA nanoparticles.

3.3. Nanoparticles stability

3.3.1. Effect of pH and NaCl solution on nanoparticles stability

As shown in Fig. 2A, the average particle size of Zein/GA nanoparticles did not change significantly compared with that of Zein/ GA-ISO nanoparticles at pH 6–8. At pH 2, the potential of nanoparticles was the highest, indicating that the stability of nanoparticles was low. At pH 4–8, the zeta potential of the Zein/GA-Iso nanoparticles increases significantly and tends to be stable. Importantly, the zeta potential of Zein/GA-Iso nanoparticles is higher than that of Zein/GA, indicating that Zein/GA-Iso has better stability.

With further increase in the salt concentration, the mean size of Zein/GA-Iso nanoparticles increased significantly ($p < 0.01$) and the stability decreased (Fig. 2B). In addition, the zeta potential also showed the same conclusion. With the increase in salt solution concentration, the zeta potential always showed a negative value, but its absolute value was getting smaller and smaller.

3.3.2. Effect of the simulated gastrointestinal conditions on nanoparticles stability

Fig. 2C reflected a significant approximate 476 nm and 865 nm of increase in the mean size of both Zein/GA and Zein/GA-Iso, respectively, at the oral phase which was in low pH of 6.8. Next, when the orally digested sample solution was mixed with the simulated gastric fluid, the mean size of Zein/GA and Zein/GA-Iso nanoparticles increased to 725 nm and 765 nm, respectively, about 5 times the initial mean size. Finally, when nanoparticles were transferred to the simulated small intestinal conditions, the mean size of nanoparticles was greatly increased, and the mean size of Zein/GA-Iso nanoparticles (1230 nm) was significantly smaller than that of Zein/GA nanoparticles (1760 nm) ($p < 0.05$). In addition, during the simulated digestion process, the absolute value of the zeta potential of Zein/GA and Zein/GA-Iso nanoparticles also decreased, which may be due to gastric juice and intestinal juice promoting the decomposition of zein, thereby reducing stability.

3.3.3. Effect of temperature and storage time on nanoparticles stability

In general, the zeta potential of Zein/GA and Zein/GA-Iso nanoparticles has little change, indicating that they have certain stability in the range of 1–90 °C. and the mean size did not change much about 131 nm–155 nm and 150 nm–168 nm, respectively, showing that nanoparticles were insensitive to temperature (Fig. 2D).

It can be observed from Fig. 2E that with the increase in the storage time, the mean size of nanoparticles increased at first and then decreased. Initially, the mean sizes of the Zein/GA and Zein/GA-Iso nanoparticles were about 124 nm and 149 nm, respectively. The mean size of Zein/GA-Iso reached maximum 1250 nm at 12 h, while that of Zein/GA reached the maximum at room temperature for 24 h, about 725 nm. After 48 h, the mean size of the two nanoparticle types gradually declined. The zeta potential of the two nanoparticles decreased at first and then stabilized at a level, that is, they remained stable after 24 h of storage in a refrigerator at 4 °C.

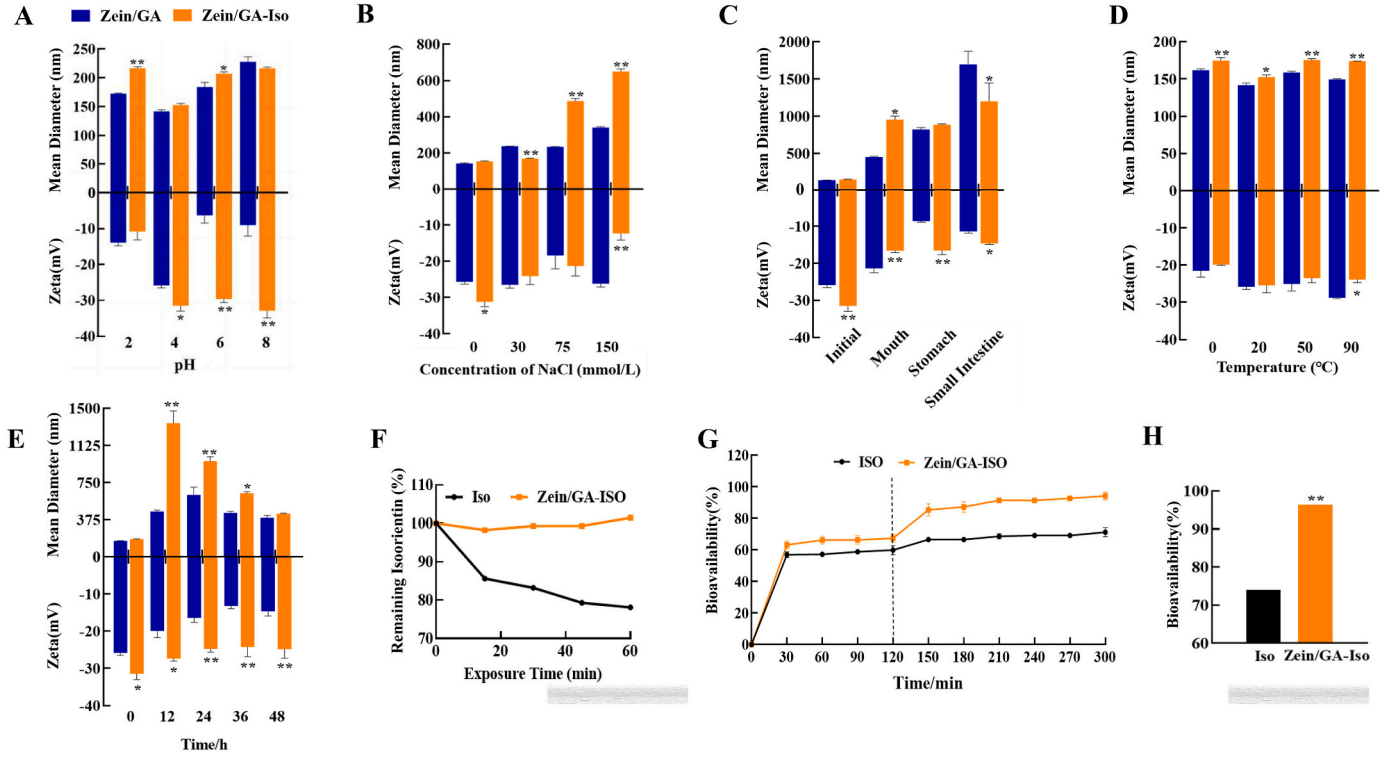

Fig. 2. Nanoparticles stability and bioaccessibility.
Mean size and zeta-potential of Zein/GA and Zein/GA-Iso nanoparticles in different pH values (A), in different concentrations of NaCl (B), in the simulated gastrointestinal digestion *in vitro* (C), at different temperature (D) and time (E). Chemical stability of Iso in Zein/GA-Iso nanoparticles under UV light (F). Bioavailability of Iso and Zein/GA-Iso nanoparticles in 300 min (G). Bioavailability of Iso and zein/GA-Iso nanoparticles (H). Values are means ± SD, $n = 3$. * $p < 0.05$, ** $p < 0.01$ *versus* Control.

3.3.4. Effect of the ultraviolet exposure on Iso in the Zein/GA-Iso nanoparticles

After ultraviolet light irradiation, the retention rate of Iso in Zein/GA-Iso nanoparticles remained 100.00%, while the retention rate of Iso in free Iso solution decreased to 76.10% (Fig. 2F), suggesting that the encapsulation of Iso in Zein/GA nanoparticles could improve the light stability of Iso.

Furthermore, both Iso and Zein/GA-Iso showed a rapid release behavior after simulating gastric digestion for 30 min, 57.5% of Iso was rapidly released into gastric juice, about 63.2% of Iso in Zein/GA-Iso nanoparticles was released into gastric juice (Fig. 2G). After 300 min, the total amount of Iso released accounted was about 95.35% and 72.32% of the Iso alone solution and Zein/GA-Iso nanoparticles, respectively. These results showed that the release behavior of Zein/GA-Iso nanoparticles to its loaded Iso was controllable, and the bioavailability of Zein/GA-Iso nanoparticles was significantly higher than that of Iso (Fig. 2H, $p < 0.01$).

3.4. In vitro antioxidant capacity

The DPPH and $ABTS^{+\cdot}$ radical scavenging capacities increased with the increase in concentration. When the concentration reached 200 μg/mL, the scavenging efficiencies of Zein/GA-Iso nanoparticles on DPPH radicals was 8.3% higher than that of Iso (Fig. 3A, $p < 0.05$), and at 40 μg/mL, there was no significant difference between the $ABTS^{+\cdot}$ radical scavenging activity of Iso and Zein/GA-Iso nanoparticles (Fig. 3B).

From Fig. 3C, the inhibition rate of Zein/GA-Iso nanoparticles on erythrocyte hemolysis gradually increased with increasing concentration. At a concentration of 200 μg/mL, the inhibition rate of red blood cell hemolysis by Zein/GA-Iso nanoparticles was significantly stronger at 40.2% compared to Iso ($p < 0.05$). Treatment with H_2O_2 resulted in dents and damages to the red blood cells, due to the lipid peroxidation destruction of cell membrane structure. The red blood cells in the control group, Zein/GA-Iso nanoparticles group showed smooth spherical surface with intact cell membranes and almost no hemolysis (Fig. 3D), indicating that Zein/GA-Iso nanoparticles were friendly towards the red blood cell.

3.5. Cytotoxicity

25 mM of Bap resulted in a notable decrease in cell viability. After incubation with Iso, the cell viability of Caco-2 and HL-7702 cells markedly increased ($p < 0.01$) by 27.35% and 47.26%, respectively, and Zein/GA-Iso nanoparticles enhanced Caco-2 and HL-7702 cell viability by 30.2% and 56.3%, respectively (Fig. 3E-H). Additionally, it can be seen from Fig. 4 that compared with control group, the amount of ROS in cells treated with Bap significantly increased, while Zein/GA-Iso nanoparticles could decrease ROS. These results showed that Zein/GA-Iso nanoparticles had little cytotoxicity, and had intracellular antioxidant capacity.

3.6. Antibacterial activity

The bacteriostatic circle and bacteriostatic rate of Iso and Zein/GA-Iso nanoparticles against *E. coli*, *S. aureus*, and *P. aeruginosa* were shown in Table S1. At a concentration of 2 mg/mL, the inhibition rates of Iso on *E. coli*, *S. aureus,* and *P. aeruginosa* were 57.20%, 51.06%, 58.39%, while the inhibition rates of Zein/GA-Iso nanoparticles were 72.73%, 69.47%, 75.31%, respectively. However, neither the control group nor the Zein/GA nanoparticles group showed any bacteriostatic effect, revealing that Zein/GA nanoparticles had negligible antibacterial activity. At the same mass concentration, both Iso and Zein/GA-Iso nanoparticles exhibited stronger inhibitory effects on *E. coli* and *P. aeruginosa* compared to *S. aureus*. Iso had a MIC for *E. coli* and *P. aeruginosa* at 1000 μg/mL, while it was higher at 1250 μg/mL for *S. aureus*. The MIC of Zein/GA-Iso nanoparticles for *E. coli* and *P. aeruginosa* was lower at 750 μg/mL, compared to about1000 μg/mL for inhibiting growth of *S. aureus* (Table S2). These results implied that both Iso and Zein/GA-Iso have better inhibitory effects on Gram-negative bacteria than Gram-positive bacteria; moreover, the inhibitory effect of Zein/GA-Iso nanoparticles is notably better than that of Iso alone.

Additionally, Zein/GA nanoparticles did not significant influence the growth of bacteria. Within the time frame from 4 to 10 h, *E. coli* (Fig. 5A), *S. aureus* (Fig. 5B), and *P. aeruginosa* (Fig. 5C) were in the logarithmic growth phase with a significantly accelerated growth rate.

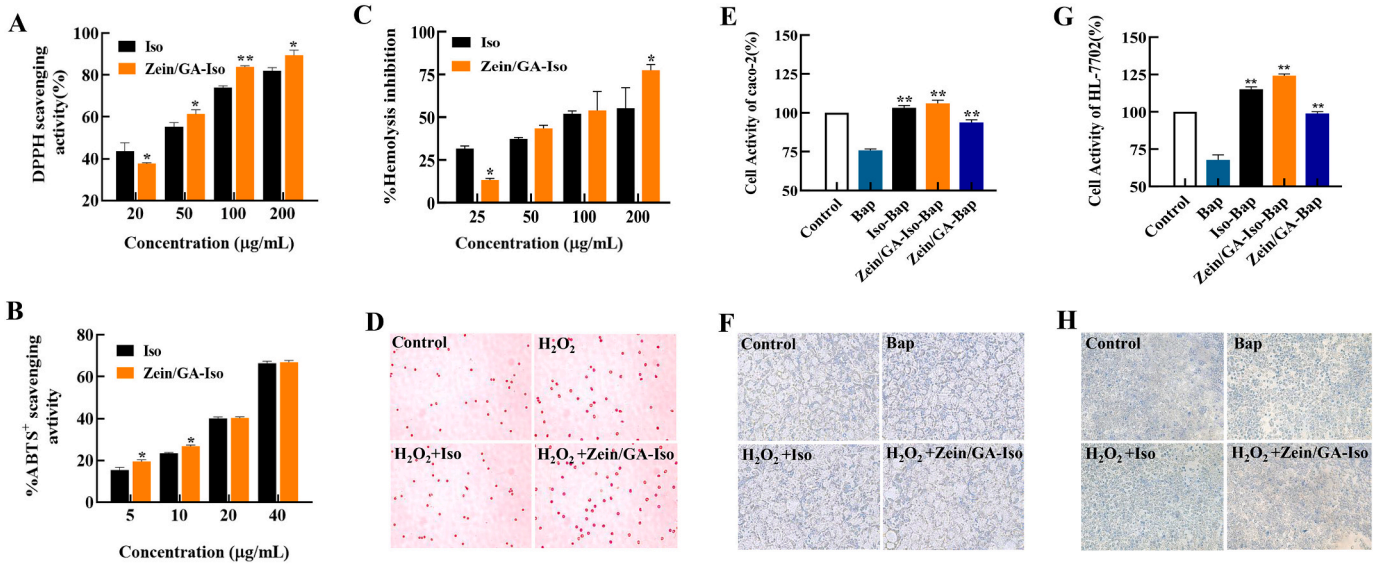

Fig. 3. Antioxidant activity, erythrocyte hemolysis and cytotoxicity of Zein/GA-Iso nanoparticles.
Scavenging ability of Iso and Zein/GA-Iso nanoparticles on (A) DPPH radicals, (B) $ABTS^{\bullet+}$ radicals. Values are means ± SD, $n = 9$. *$p < 0.05$, **$p < 0.01$ *vs* Iso group. (C) Inhibitive effect of Iso and Zein/GA-Iso nanoparticles on H_2O_2 (200 μg/mL) induced erythrocyte hemolysis. (D) Micrograph of erythrocyte morphologic changes were also observed by optic microscope (original magnification of 100×). Effect of Iso, Zein/GA and Zein/GA-Iso nanoparticles on cell viability of (E) Caco-2 cell and (F) HL-7702 cell exposed Bap, respectively. Values are means± SD, n = 9. * $p < 0.05$, ** $p < 0.01$ *versus* Control. Micrograph of Caco-2 cell (G) and HL-7702 cell (H), (original magnification of 100×).

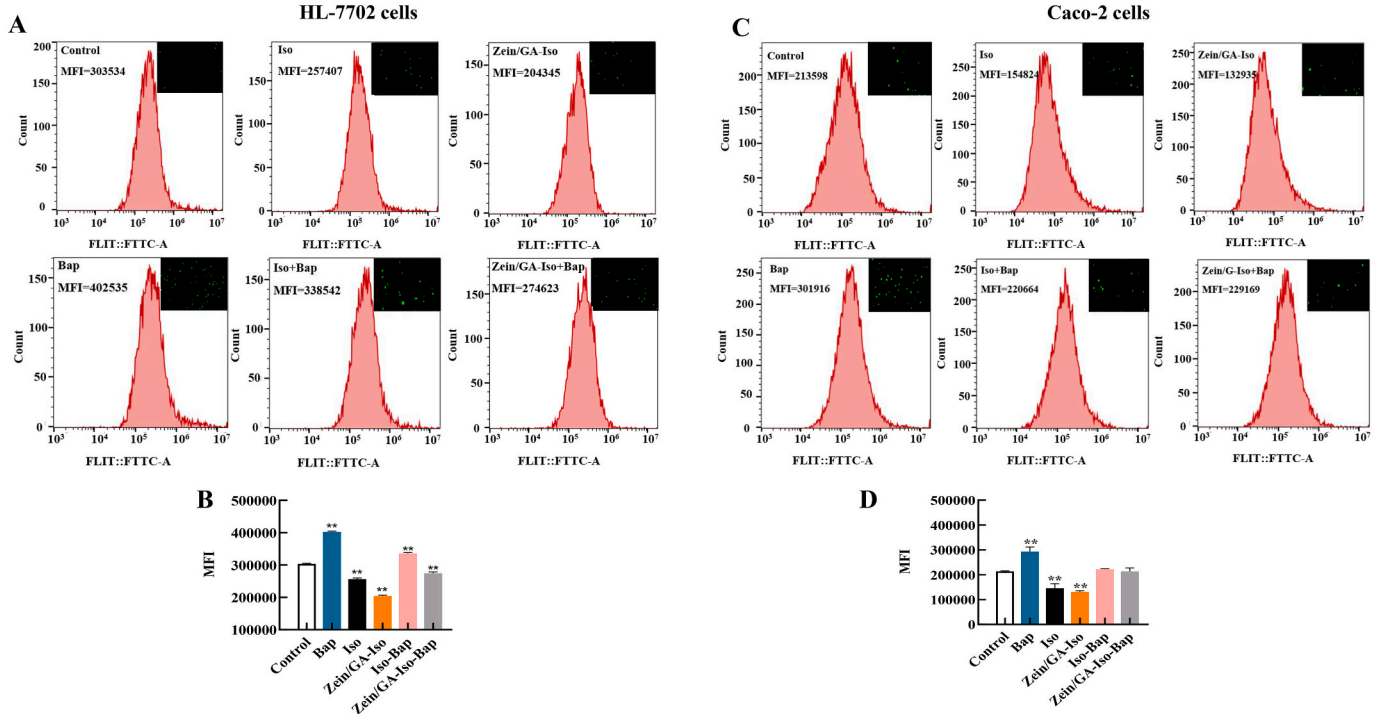

Fig. 4. Effect of Zein/GA-Iso nanoparticles on Bap-stimulated ROS of Caco-2 cells and HL-7702 cells.
ROS were examined by Flow cytometer (A, C) and Fluorescence microscope (B, D), MFI refers to the mean fluorescence intensity in flow cytometry analysis.

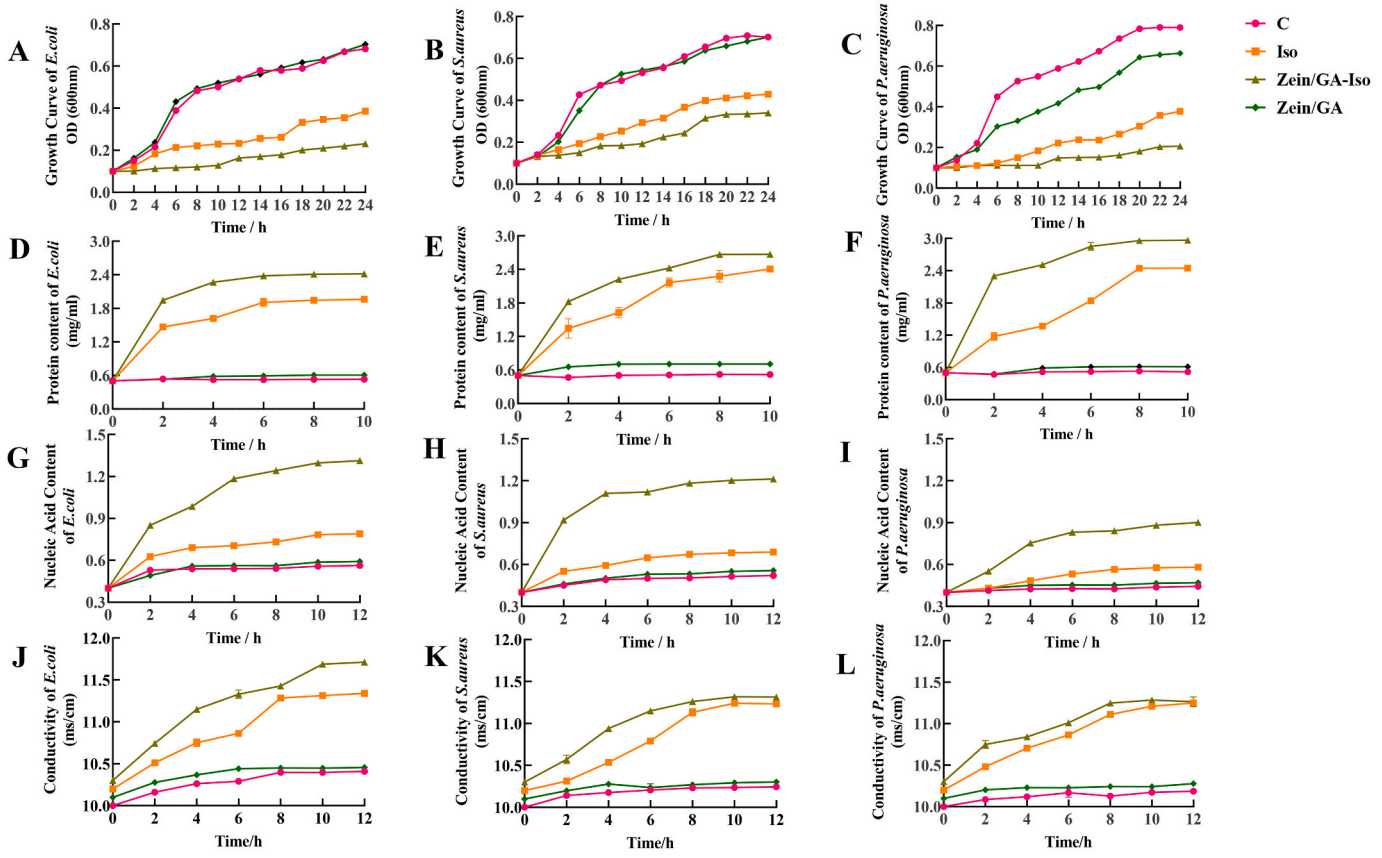

Fig. 5. Antibacterial activity of Zein/GA-Iso nanoparticles.
Effect of Iso, Zein/GA and Zein/GA-Iso nanoparticles on the growth curve (A-C), the extracellular protein content (D—F), the extracellular nucleic acid content (G-I) and conductivity (J-L) of *E. coli*, *S. aureus* and *P. aeruginosa*. *P. aeruginosa*, respectively.

However, in Iso and Zein/GA-Iso nanoparticles group, the growth rate of these bacteria remained suppressed, indicating that Iso and Zein/GA-Iso nanoparticles inhibited or disrupted the growth cycle of bacteria. After 10 h of culture, the bacterial growth rates in Zein/GA nanoparticles group were still at a low levels, and the number of bacteria also was lower than that of Iso group.

Furthermore, damage to the cell membrane structure of microorganisms results in a large number extravasation of intracellular protein, and they are detected in cell culture or tissue extracts. There was no significant difference in the soluble protein leak of bacteria between control and Zein/GA nanoparticles group. Compared with control group, the content of protein leakage was significantly increased by Iso and Zein/GA-Iso nanoparticles. However, the amount of protein leakage in Iso group was always lower than that in Zein/GA-Iso nanoparticles group (Fig. 5D-F). The same results were observed in the nucleic acid leakage (Fig. 5G-I) and conductivity (Fig. 5J-L) in the bacterial suspension.

As shown in Fig. 6, both *E. coli* and *P. aeruginosa* exhibited a rod shape, while *S. aureus* showed a grape string shape in the control and Zein/GA group. After Iso treatment, certain wrinkle and damage to the cell membranes of *E. coli* and *P. aeruginosa* were observed, with the surface of *S. aureus* appearing rough and partially sunken inward. Zein/GA-Iso nanoparticles caused more severe unevenness and damaged to the surface of *E. coli*, while *S. aureus* and *P. aeruginosa* displayed stickiness with noticeable surface holes. These results suggested that loading Iso onto Zein/GA-Iso nanoparticles significantly enhanced the antibacterial ability of Iso.

3.7. Preservation effect of Zein/GA-Iso nanoparticles on chilled meat

To further evaluate the antibacterial effect of Zein/GA-Iso nanoparticles, they were used for soaking treatment of chilled pork. As shown in Fig. 7A, with increasing storage time, the color of pork changed from bright red to dark and dull, however, no discernible change was observed in the zein/GA-Iso nanoparticles treated group. The color difference meter also revealed that the a* and L* values of the samples treated with zein/GA-Iso nanoparticles were significantly higher than those in the control group during 2–4 days, whereas b* value remained consistently lower throughout (Fig. 7B). Simultaneously, pH value of pork in the zein/GA-Iso nanoparticles treated group was constantly lower than that in the control group, this difference became significant after 4 days. During storage period, the drip loss decreased for pork samples treated with Iso or Zein/GA-Iso nanoparticles compared to control group, however it still remained higher than that in control group. Similarly, after day 4, TVB-N value as was as the total number of colonies were significantly lower for Zein/GA-Iso nanoparticles group compared to control group, (Fig. 7C, D). In conclusion, these findings indicated that stronger bacteriostatic potential possessed by Zein/GA-Iso nanoparticles.

4. Discussion

The construction of nano-nutrient delivery carriers for proteins and polysaccharides is an effective means of enhancing the efficacy of bioactive, such as Zein/Chitosan-α-tocopherol (Luo et al., 2011), Zein/Chitosan-resveratrol (Guo et al., 2015). In this experiment, the anti-solvent precipitation method was used to prepare small-size Zein/GA nanoparticle, and the loading efficiency of Iso in Zein/GA-Iso nanoparticles was 67.6%, indicating that the nanoparticle synthesis method and flavonoid loading proportion used in this study were effective.

The mean size and zeta potential are critical to the nanocarrier system, as they not only affect the activity of the loaded components but also impact the stability of the system *in vitro* or *in vivo*. The mean sizes of Zein/GA nanoparticles and Zein/GA-Iso nanoparticles were 122 nm and 142 nm, respectively, both exhibiting a spherical shape. When electrostatic interaction occurs during the formation of Zein/GA nanoparticles, zeta shows a negative charge, implying that GA fully wraps Zein and forms a protective shell on the surface of zein (Wang et al., 2021). Consistent with this description, the zeta potential of Zein/GA nanoparticles was −25.3 mV, while Zein/GA-Iso nanoparticles showed a lower zeta potential (−30.1 mV), which may be attributed to enhance the stability of nanoparticles due flavonoid presence (Li et al., 2019). Hydrogen bond interactions along with electrostatic force and hydrophobic force play key roles in synthesizing Zein/GA nanoparticles and Zein/GA-Iso nanoparticles. Iso exhibits hydrophobic properties. Surprisingly, the contact angle of Zein/GA-Iso nanoparticles (27.3°) was higher than that of Iso (38.9°). The possible reason was attributed to GA adsorbing onto the Zein's surface, wrapping Zein with poor hydrophilicity inside, resulting in enhanced hydrophilicity of nanoparticles. In addition, the hydrophilicity of Zein/GA-Iso was stronger than that of

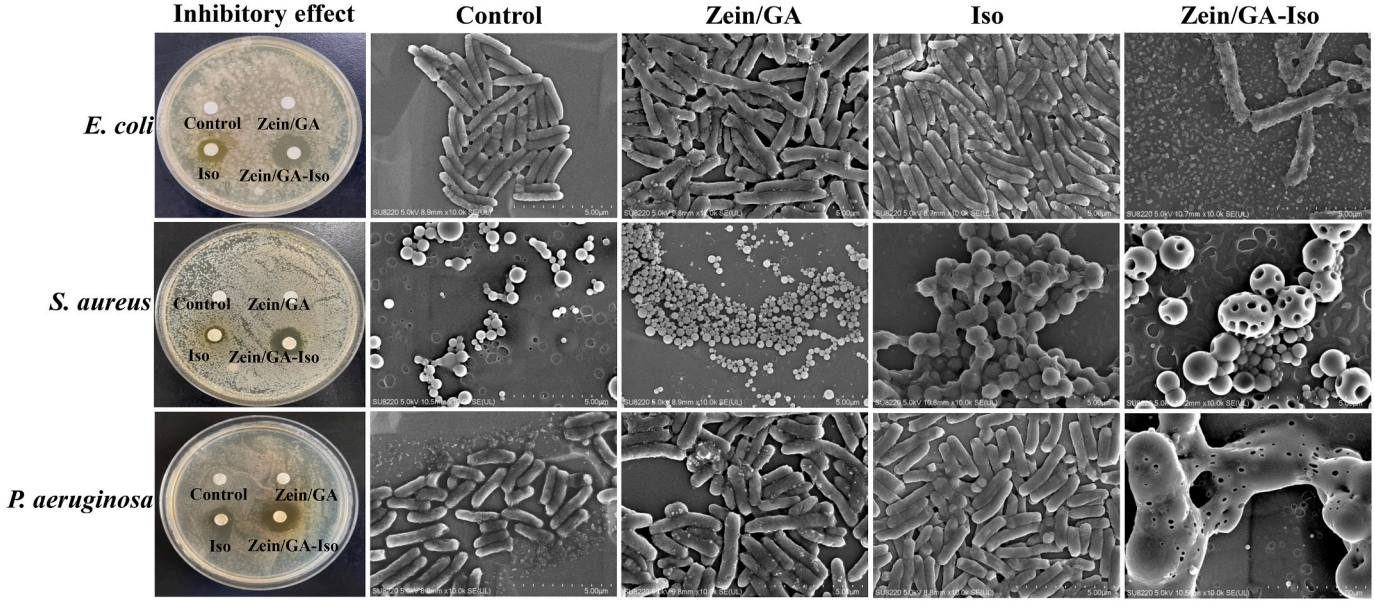

Fig. 6. Inhibitory effects of nanoparticles on bacteria and structural characteristics of bacteria.
Effects of Iso and Zein/GA-Iso nanoparticles on bacterial colony and morphological structure of *E. coli*, *S. aureus* and *P. aeruginosa*.

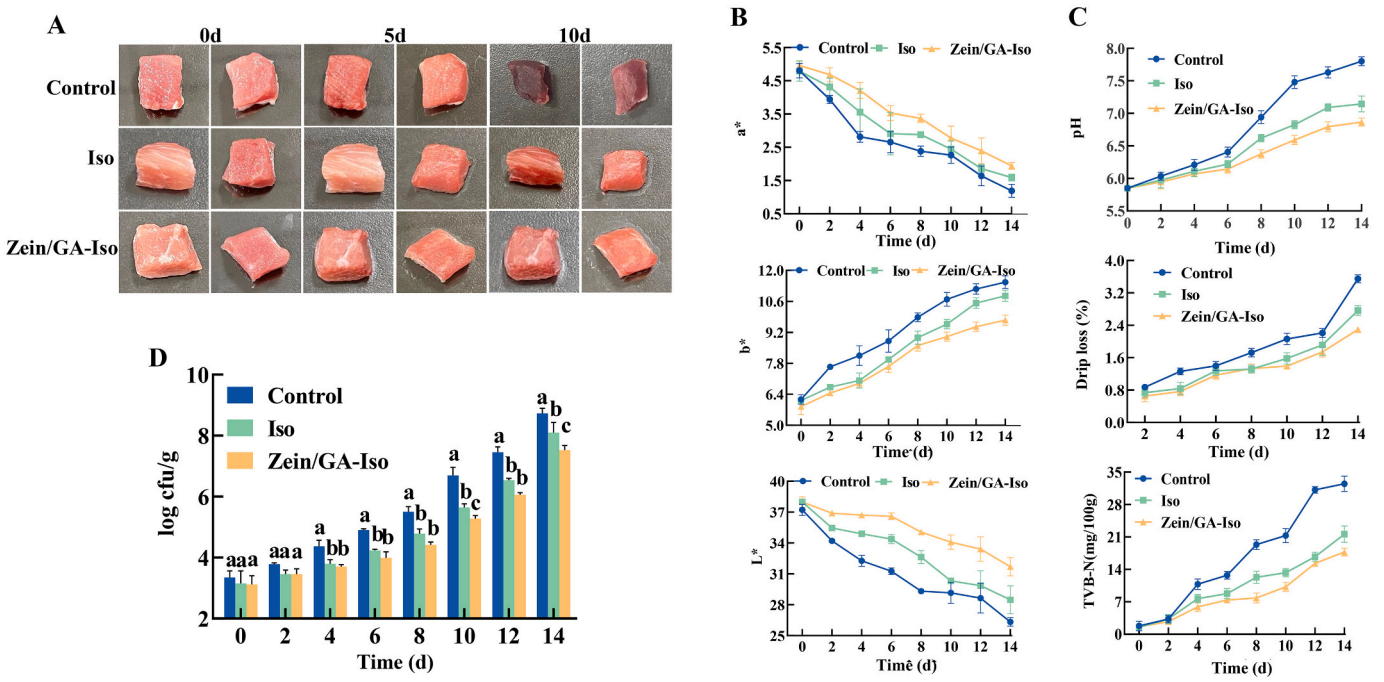

Fig. 7. Preservation effect of Zein/GA-Iso nanoparticles on chilled pork.
The color (A), the a*, L* and b* values (B), the pH value, the water retention capacity and the TVB-N value(C, D).

Zein/GA nanoparticles, indicating successfully embedding of Iso in Zein/GA nanoparticles and distribution of GA with good hydrophilicity in the outer shell of nanoparticles, theybe improving the hydrophilicity of Iso and Zein/GA nanoparticles. This improvement in solubility provides a solid foundation for the application of Iso.

The stability of Zein/GA-Iso nanoparticles greatly influences their application in food processing, storage, cooking, or passage through the gastrointestinal tract. We found high stability of both Zein/GA and Zein/GA-Iso nanoparticles at pH 4 (Fig. 2A), presumably due to the low net charge on the surface of Zein. When the pH of system approached the isoelectric point (pH = 6.5) of Zein, electrostatic repulsion between nanoparticles decreased, leading to an increasing tendency for aggregation and larger mean size (Tokle et al., 2010). Moreover, as salt solution concentration increased to 75-150 M, there was a gradual increase in the mean size for both types of nanoparticle (Fig. 2B). This could be attributed to an increase in counterions wihtin the solution, which neutralized the charge of nanoparticles and weakened the electrostatic force between them through electrostatic shielding, resulting in some degree of aggregation of nanoparticles. These findings suggest that while proteins and polysaccharides can resist low concentrations of salt ions through their electrostatic interaction force, this force is relatively wea (Yuan et al., 2023).

Iso was prone to photolysis under UV light, which led to a decrease in activity. After loading Iso on Zein/GA nanoparticles, the exposure amount of Iso under UV light decreases, and no photolysis of Iso was found (Fig. 2F). It can be speculated that was the influence of light scattering and absorption effects and the slow release of a small part of Iso from Zein/GA-Iso nanoparticles under UV light (Iris, Gabriel, & David, 2015).

Furthermore, the mean size of nanoparticles significantly increased during the oral phase, which may be attributed to the electrostatic shielding effect and the presence of mucin-promoting protein bridging and flocculation, and the decrease in the absolute value of nanoparticles potential was attributed to mucin binding through electrostatic interaction (Chang and McClements, 2016). In the simulated gastric and small intestinal digestive juices, there was a significant increase in mean size and a decrease in the absolute value of zeta potential. This could be due to the gastrointestinal tract pH (pH = 7) being close to the isoelectric points of Zein (PI = 7), as well as neutralization of surface charge by NaCl and $CaCl_2$, resulting in electrostatic shielding. In addition, pepsin and trypsin continuously hydrolyze part of Zein, leading to an increase in mean size of nanoparticles. The higher release rate during the gastric digestion stage may be attributed to a fact that Zein/GA-Iso nanoparticles having better hydrophilicity than Iso, allowing for rapid dissolution in gastric juice, which was consistent with water contact angle. The release rate of Zein/GA-Iso nanoparticles during the intestinal phase was higher than that of Iso, due to the dissolution of GA under neutral pH conditions facilitating Zein hydrolysis by trypsin. The higher release rate may also result from complexation between digestive enzymes and peptides present in gastrointestinal juice (Wu et al., 2020).

The significant enhancement observed in the antioxidant capacity of Zein/GA-Iso nanoparticles may be due to their improved hydrophilicity. That was because when the surface of the nanoparticles become more hydrophilic, containing more (-OH) or other polar groups, they are better able to interact with water molecules, which helps to absorb and transfer oxygen around them, theybe enhancing their antioxidant properties (Chen et al., 2021). It was reported that nanoparticles have low toxicity and safety (Anwar et al., 2019). This study also found that Zein/GA-Iso nanoparticles obviously inhibited erythrocyte hemolysis, and there was no significant cytotoxicity of Zein/GA-Iso nanoparticles on Caco-2 cells and HL-7702 cells, possessing a good bio-safety (Fig. 3E-H).

Furthermore, the antibacterial ability of Iso was enhanced by loading it onto Zein/GA nanoparticles. Zein/GA-Iso nanoparticles achieved a bacteriostatic effect by disrupting the integrity of bacterial cell membrane, leading to extravasation of intracellular materials such as proteins, DNA, Na^+, and K^+, which resulted in an imbalance of osmotic pressure inside and outside the cell membrane, causing the cell to shrink or swell (Yi et al., 2019). SEM images also confirmed that Zein/GA-Iso nanoparticles exhibited better antibacterial effects than Iso alone, due to their small size. Zein/GA-Iso nanoparticles could create pores on the surface of bacterial cell membrane and penetrate into the bacteria. Some studies have shown that treatment with silver nanoparticles can destroy cellular integrity of *Pseudomonas aeruginosa*, causing some bacteria to

become swollen or atrophied, while experiencing deformation or rupture of their cell membrane and release of cellular contents (Liao et al., 2019; Pan et al., 2019). In addition, the present study discovered that Zein/GA-Iso nanoparticles significantly delayed increase in pH value, TVB-N levels and the colony count in chilled pork, while maintaining continuous color protection properties, suggesting that Zein/GA-Iso nanoparticles have strong bacteriostatic effect.

5. Conclusion

Zein/GA-Iso nanoparticles were successfully prepared using the classical antisolvent precipitation method. They exhibited a spherical shape with uniform distribution, and had the smallest mean size (149 nm) at pH 4, and possessed excellent stability in salt solution ranging from 0 to 30 M as well as temperatures up to 90 °C. Importantly, Zein/GA-Iso nanoparticles showed good solubility in water and strong antibacterial capacity with no significant cytotoxicity. Nanoparticles encapsulation could improve the antioxidant and antibacterial activity of Iso *in vitro*, and exhibit a better fresh-keeping effect on cold meat. These results provided references for expanding the application of Iso, especially in the application of food preservation.

Ethical statement

Animal protocols were approved by the Scientific Ethics Professional Committee of Shaanxi Normal University Academic Committee (Xi'an, Shaanxi, China). All animals were kept in a pathogen-free environment and fed *ad lib*. The procedures for care and use of animals were approved by the Ethics Committee of the Laboratory Animal Center of Shaanxi Normal University and all applicable institutional and governmental regulations concerning the ethical use of animals were followed. To minimize suffering, the animals were handled with compassion.

CRediT authorship contribution statement

Yuxia Yang: Writing – review & editing. **Yingyu Jia:** Writing – review & editing, Software, Methodology. **Meng Zhang:** Writing – original draft, Investigation. **Ying Luo:** Resources, Methodology, Investigation. **Zhong Zhang:** Validation, Supervision. **Wanqiang Wu:** Supervision, Project administration, Funding acquisition. **Li Yuan:** Writing – review & editing, Visualization, Funding acquisition.

Declaration of competing interest

The authors declare that they have no known competing financial interests or personal relationships that could have appeared to influence the work reported in this paper.

Data availability

Data will be made available on request.

Acknowledgement

This work was financially supported by the National Natural Science Foundation of China (31972183, 82103844), the Regional Innovation Capability Guidance Program of Shaanxi Province (2022QFY09-03), and the Training Program of Excellent Youth Innovation Team (GK202401006).

Appendix A. Supplementary data

Supplementary data to this article can be found online at https://doi.org/10.1016/j.fochx.2024.101604.

References

Ambika, S., & Sundrarajan, M. (2015). Antibacterial behaviour of *Vitex negundo* extract assisted ZnO nanoparticles against pathogenic bacteria. *Journal of Photochemistry and Photobiology, B: Biology, 146*, 52–57. https://doi.org/10.1016/j.jphotobiol.2015.02.020

Antônio, E., Khalil, N. M., & Mainardes, R. M. (2016). Bovine serum albumin nanoparticles containing quercetin: Characterization and antioxidant activity. *Journal of Nanoscience and Nanotechnology, 16*(2), 1346–1353. https://doi.org/10.1166/jnn.2016.11672

Anwar, A., Masri, A., Rao, K., Rajendran, K., Khan, N. A., Shah, M. R., & Siddiqui, R. (2019). Antimicrobial activities of green synthesized gums-stabilized nanoparticles loaded with flavonoids. *Scientific Reports, 9*(1), 3122. https://doi.org/10.1038/s41598-019-39528-0

Chang, Y., & McClements, J. D. (2016). Characterization of mucin-lipid droplet interactions: Influence on potential fate of fish oil-in-water emulsions under simulated gastrointestinal conditions. *Food Hydrocolloids*, 425–433. https://doi.org/10.1016/j.foodhyd.2015.12.034

Chen, C., Zhao, M., & Sun, W. Z. (2021). Antioxidant activity and electron donor capacity of tyrosine-containing dipeptides in liposomes. *Food Science, 11*, 1–7. https://doi.org/10.7506/spkx1002-6630-20200617-232

Gagliardi, A., Voci, S., Salvatici, M. C., Fresta, M., & Cosco, D. (2021). Brij-stabilized zein nanoparticles as potential drug carriers. *Colloids and Surfaces. B, Biointerfaces, 201*, Article 111647. https://doi.org/10.1016/j.colsurfb.2021.111647

Gali, L., Bedjou, F., Ferrari, G., & Donsì, F. (2022). Formulation and characterization of zein/gum arabic nanoparticles for the encapsulation of a rutin-rich extract from Ruta chalepensis L. *Food Chemistry, 367*, Article 129982. https://doi.org/10.1016/j.foodchem.2021. 129982

Gao, J., Liang, H., Li, S., & Zhou, B. (2021). Development of zein/soluble soybean polysaccharide nanoparticle-stabilized Pickering emulsions. *Journal of Food Science, 86*(5), 1907–1916. https://doi.org/10.1111/1750-3841.15730

Guo, L., Peng, Y., Li, Y., Yao, J., Zhang, G., Chen, J., Wang, J., & Sui, L. (2015). Cell death pathway induced by resveratrol-bovine serum albumin nanoparticles in a human ovarian cell line. *Oncology Letters, 9*(3), 1359–1363. https://doi.org/10.3892/ol.2015. 2851

Iris, J. J., Gabriel, D. P., & David, J. M. (2015). Encapsulation of resveratrol in biopolymer particles produced using liquid antisolvent precipitation. Part 2: Stability and functionality. *Food Hydrocolloids, 49*, 127–134. https://doi.org/10.1016/j.foodhyd.2015.02.038

Li, H., Wang, D., Liu, C., Zhu, J., Fan, M., Sun, X., Wang, T., Xu, Y., & Cao, Y. (2019). Fabrication of stable zein nanoparticles coated with soluble soybean polysaccharide for encapsulation of quercetin. *Food Hydrocolloids, 8*, 342–351. https://doi.org/10.1016/j.foodhyd.2018.08.002

Liao, S., Zhang, Y., Pan, X., Zhu, F., Jiang, C., Liu, Q., Cheng, Z., Dai, G., Wu, G., Wang, L., & Chen, L. (2019). Antibacterial activity and mechanism of silver nanoparticles against multidrug-resistant Pseudomonas aeruginosa. *International Journal of Nanomedicine, 14*, 1469–1487. https://doi.org/10.2147/IJN.S191340

Lim, J. H., Park, H. S., Choi, J. K., Lee, I. S., & Choi, H. J. (2007). Isoorientin induces Nrf2 pathway-driven antioxidant response through phosphatidylinositol 3-kinase signaling. *Archives of Pharmacal Research, 30*(12), 1590–1598. https://doi.org/10.1007/BF02977329

Lin, X., Wei, J., Chen, Y., He, P., Lin, J., Tan, S., Nie, J., Lu, S., He, M., Lu, Z., & Huang, Q. (2016). Isoorientin from Gypsophila elegans induces apoptosis in liver cancer cells via mitochondrial-mediated pathway. *Journal of Ethnopharmacology, 187*, 187–194. https://doi.org/10.1016/j.jep.2016.04.050

Luo, Y., Zhang, B., Whent, M., Yu, L. L., & Wang, Q. (2011). Preparation and characterization of zein/chitosan complex for encapsulation of α-tocopherol, and its in vitro controlled release study. *Colloids and Surfaces. B, Biointerfaces, 85*(2), 145–152. https://doi.org/10.1016/j.colsurfb.2011.02.020

Pan, Y., Zheng, L. B., Mao, Y., Wang, J., Lin, L. S., Su, Y. Q., & Li, Y. (2019). The antibacterial activity and mechanism analysis of piscidin 5 like from Larimichthys crocea. *Developmental and Comparative Immunology*, 43–49. https://doi.org/10.1016/j.dci.2018.10.008

Song, J., Sun, C., Zhang, J., Xiong, Z., & Fang, Y. (2020). Fabrication, characterization, and formation mechanism of Zein-Gum Arabic nanocomposites in aqueous ethanol solution with a high ethanol content. *Journal of Agricultural and Food Chemistry, 46*, 13138–13145. https://doi.org/10.1021/acs.jafc.9b08179

Tokle, T., Lesmes, U., & McClements, D. J. (2010). Impact of electrostatic deposition of anionic polysaccharides on the stability of oil droplets coated by lactoferrin. *Journal of Agricultural and Food Chemistry, 58*(17), 9825–9832. https://doi.org/10.1021/jf101833z

Wang, X., Yuan, L., Deng, H., & Zhang, Z. (2021). Structural characterization and stability study of green synthesized starch stabilized silver nanoparticles loaded with isoorientin. *Food Chemistry, 338*, Article 127807. https://doi.org/10.1016/j.foodchem. 2020. 127807

Wang, Y., & Padua, G. W. (2010). Formation of zein microphases in ethanol-water. *Langmui, 26*(15), 12897–12901. https://doi.org/10.1021/la101688v

Wiegand, I., Hilpert, K., Hancock, R., & E. W.. (2008). Agar and broth dilution methods to determine the minimal inhibitory concentration (MIC) of antimicrobial substances. *Nature Protocols, 2*, 163–175. https://doi.org/10.1038/nprot.2007.521

Wu, W., Kong, X., Zhang, C., Hua, Y., Chen, Y., & Li, X. (2020). Fabrication and characterization of resveratrol-loaded gliadin nanoparticles stabilized by gum Arabic and chitosan hydrochloride. *LWT, 129*, Article 109532. https://doi.org/10.1016/j.lwt.2020. 109532

Yi, J., Zhang, Y., Lin, W., Niu, B., & Chen, Q. (2019). Effect of polyhexamethylene biguanide functionalized silver nanoparticles on the growth of *Staphylococcus aureus*.

FEMS Microbiology Letters, 366(4), Article fnz036. https://doi.org/10.1093/femsle/fnz036

Yuan, L., Wu, Y., Ren, X., Liu, Q., Wang, J., & Liu, X. (2014). Isoorientin attenuates lipopolysaccharide-induced pro-inflammatory responses through down-regulation of ROS-related MAPK/NF-κB signaling pathway in BV-2 microglia. *Molecular and Cellular Biochemistry, 386*(1–2), 153–165. https://doi.org/10.1007/s11010-013-1854-9

Yuan, Y., Ma, M., Wang, D., & Xu, Y. (2023). A review of factors affecting the stability of zein-based nanoparticles loaded with bioactive compounds: From construction to application. *Critical Reviews in Food Science and Nutrition, 63*(25), 7529–7545. https://doi.org/10.1080/10408398.2022.2047881

Zhang, Y., Xu, M., Zhang, X., Hu, Y., & Luan, G. (2022). Application of zein in gluten-free foods: A comprehensive review. *Food Research International, 160*, 11172. https://doi.org/10.1016/J.FOODRES.2022.111722